HHS Public Access

Author manuscript

HVAC&R Res. Author manuscript; available in PMC 2015 October 30.

Published in final edited form as:

HVAC&R Res. 2013 ; 19(8): 962–973. doi:10.1080/10789669.2013.838990.

Airborne exposure patterns from a passenger source in aircraft cabins

James S. Bennett[1,*], **Byron W. Jones**[2], **Mohammad H. Hosni**[2], **Yuanhui Zhang**[3], **Jennifer L. Topmiller**[1], and **Watts L. Dietrich**[1]

[1]National Institute for Occupational Safety and Health, Centers for Disease Control and Prevention, U.S. Department of Health and Human Services, 4676 Columbia Parkway, MS R5, Cincinnati, OH 45226-1998, USA

[2]Department of Mechanical and Nuclear Engineering, Kansas State University, Manhattan, KS, USA

[3]Department of Agricultural and Biological Engineering, University of Illinois at Urbana-Champaign, Urbana, IL, USA

Abstract

Airflow is a critical factor that influences air quality, airborne contaminant distribution, and disease transmission in commercial airliner cabins. The general aircraft-cabin air-contaminant transport effect model seeks to build exposure-spatial relationships between contaminant sources and receptors, quantify the uncertainty, and provide a platform for incorporation of data from a variety of studies. Knowledge of infection risk to flight crews and passengers is needed to form a coherent response to an unfolding epidemic, and infection risk may have an airborne pathogen exposure component. The general aircraf-tcabin air-contaminant transport effect model was applied to datasets from the University of Illinois and Kansas State University and also to case study information from a flight with probable severe acute respiratory syndrome transmission. Data were fit to regression curves, where the dependent variable was contaminant concentration (normalized for source strength and ventilation rate), and the independent variable was distance between source and measurement locations. The data-driven model showed exposure to viable small droplets and post-evaporation nuclei at a source distance of several rows in a mock-up of a twin-aisle airliner with seven seats per row. Similar behavior was observed in tracer gas, particle experiments, and flight infection data for severe acute respiratory syndrome. The study supports the airborne pathway as part of the matrix of possible disease transmission modes in aircraft cabins.

[*]Corresponding author jbennett@cdc.gov.

James S. Bennett, PhD, is Research Engineer. **Byron W. Jones, PhD, PE**, Member ASHRAE, is Professor and Member of the FAA Air Transportation Center of Excellence for Airliner Cabin Environment Research. **Mohammad H. Hosni, PhD, PE**, Fellow ASHRAE, is Professor and Member of the FAA Air Transportation Center of Excellence for Airliner Cabin Environment Research. **Yuanhui Zhang, PhD, PE**, Fellow ASHRAE, is Professor. **Jennifer L. Topmiller** is Control Technology Team Leader. **Watts L. Dietrich** is Co-Op Student.

Introduction

National Institute for Occupational Safety and Health (NIOSH) research into the aircraft cabin environment began with a request from the Federal Aviation Administration (FAA) to study health effects among aircraft crews. A review of previous studies showed that female flight attendants may be at increased risk of adverse reproductive outcomes (Waters et al. 2000). Exposure assessments and epidemiologic studies in the areas of radiation and cabin air quality studies followed (Waters et al. 2000; Grajewski et al. 2002; Whelan et al. 2002). Difficulties in conducting studies in the passenger aircraft cabin environment during flight led to the decision that further work be done using realistic cabin mock-ups and computational fluid dynamics (CFD) to understand the behavior of any air contaminants present.

The aircraft cabin environment is maintained during flight by the environmental control system (ECS). It is no small accomplishment to provide a safe atmosphere at cruise altitude, say 35,000 ft. In addition to pressurization, the ECS provides clean outside air to the cabin, which has a high occupancy density compared to, for example, office buildings and classrooms. In newer aircraft, approximately 50% of the air supplied to the cabin has been recirculated and passed through a high-efficiency particle air (HEPA) filter, with the remaining supply volume coming from the outside. The ECS is designed to use the length of the cabin as a plenum, so that air is supplied and exhausted at a velocity that is constant with respect to the length of the plane. Also, the direction of flow out of the supply and into the exhaust slots is in the seat-row direction, perpendicular to the aisle. The movement of air between seat rows is thus minimized in the ECS design concept.

While the ECS is intended to create airflow from the supply outlet that is two-dimensional, the flow in the open space of the cabin is freer and somewhat turbulent, insofar as it is characterized by fluctuations in velocity (speed and direction). Moreover, the supply flow in a real operating aircraft can be three dimensional and time varying. Liu et al. (2012) conducted experiments in the first-class cabin of an MD-82 and reported that "… velocity magnitude, velocity direction, and turbulence intensity varied significantly from one slot opening to another" (p. 33–44).

A flow can be deconstructed into its Reynold's-averaged velocity components:

$$U(t)=\overline{U}+u(t), \quad (1)$$

where each instantaneous component, $U(t)$, is the sum of a time average and a fluctuation with a time average of zero (Hinze 1975). Air contaminants, such as small droplets from an exhaled breath or a cough, are transported by the fluctuations, even though the average of the fluctuations is zero. The ECS then creates two competing processes, one that is intended and another that is perhaps impossible to avoid— (1) removal of potentially contaminated cabin air into the exhaust and replacement with clean air and (2) movement of contaminants within cabin air by flow fluctuations. Fluctuations are present, even in the hypothetical absence of obstructions, moving bodies, and thermal plumes.

Airflow and contaminant transport research has taken place in collaboration with many expert partners. The data generated by collaborations have been flow fields measured by experiments with realistic mock-ups or calculated using CFD. The flow fields have consisted of velocity, turbulence parameters, and either gas or aerosol contaminant concentration.

CFD simulations took place in collaboration with a commercial airliner manufacturer (Lin et al. 2005a, 2005b). At the University of Illinois, experiments in a five-row, twin-aisle mock-up, shown in Figure 1, delivered volumetric particle tracking velocimetry (VPTV) images of cabin flow seeded with helium bubbles and tracer gas (CO_2) concentration fields generated by three source locations and three ventilation rates (Sun et al. 2005; Wang et al. 2006; Wei et al. 2009; Zhang et al. 2005). Sandia National Labs provided a massively parallel computing platform for Lin et al. (2006) to complete the CFD simulations, including large eddy simulation (LES). Sandia also provided NIOSH with advice on and evaluation of the cabin airflow research and suggested that tracer gas experiments would be useful. Data in a large, wide-body airliner, including velocity and turbulence fields, were gathered by the University of Tennessee, at the FAA Aero-medical Research Institute (Garner et al. 2003). They also created detailed CFD simulations of the fluctuating cabin flows in that aircraft and in a corporate jet (Baker et al. 2000). NIOSH provided a review of Tennessee's report to the FAA (Baker et al. 2006).

Kansas State University (KSU) has conducted experiments in an 11-row, twin-aisle mock-up. Purdue University has done large-scale CFD simulations, including the wake effect of a body moving in the aisle (Rai and Chen 2012; Mazumdar et al. 2011). Some collaborators, including KSU (Hosni and Jones 2001) and Purdue, and NIOSH researchers were involved in research projects sponsored by ASHRAE and the development of an ASHRAE standard for aircraft cabin ventilation.

Much work has been done; yet the role of ventilation in controlling disease transmission in aircraft cabins remains opaque. There is consensus that the issue is complex due to the many variables involved. Figure 2 diagrams possible modes of transmission and variables discussed during the 2009 Trans-portation Research Board (TRB) conference (TRB 2012). The airflow-related portion of disease transmission was recently addressed, through deterministic and probabilistic methods, by Gupta et al. (2012).

In an effort to pull immediately useful information out of the detailed, high-quality studies done to date, a simple model and a modeling framework are presented here. The general aircraft-cabin air-contaminant transport effect (GAATE) model seeks to build exposure-spatial relationships between contaminant sources and receptors, quantify the uncertainty, and provide a platform for incorporation of future studies. To put this model in context, of the many variables presented in Figure 2, the GAATE model involves only the five variables indicated by the lighter gray elements of the diagram.

Knowledge of the infection risk to flight crews and passengers is needed to form a coherent response to an unfolding epidemic. An essential part of infection risk is exposure, and exposure may have an airborne component. The infection with severe acute respiratory

syndrome (SARS) of flight attendants on a flight from Hong Kong to Beijing on March 15, 2003, is evidence of the risk faced by these workers, who in some situations find themselves in the role of first responders. Moreover, the Association of Flight Attendants (AFA) asked the FAA for protection from SARS (AFA-WCA 2003). The goal of the GAATE model, then, is to provide useful information to authorities for addressing exposure incidents involving SARS, avian flu, H1N1, and other potentially lethal agents and to provide guidance to emergency response personnel.

Methods

Combining datasets

The GAATE model can be thought of as a meta-model, that is, a model built from other models or studies. As such, the first step is solicitation of contaminant transport data for aircraft cabin environments from research partners. These datasets must be placed on a common footing, normalized to remove sources of meaningless variability. The large meta-dataset thus formed is amenable to statistical analysis. Variables that must be normalized are emission rate of the contaminant source and air change rate of the cabin. The ratio of these two terms is, under steady-state conditions and perfect mixing, the contaminant concentration. However, the emission rate is often not constant or precisely known in aircraft cabin experiments. Consider the release of a known mass of powder, in view of the difficulty of expression as a rate. This circumstance led to using a data-driven reference concentration.

There is no location within the cabin where the steady-state, perfectly mixed concentration can be measured. Two imperfect substitutes for this idealized quantity are the average of concentrations at all measurement locations and the maximum measured concentration. These variables are designated C_{AVE} and C_S, respectively. Because each of these has its strengths and weaknesses, a reference concentration was defined as the average of C_{Ave} and C_S in the interest of robustness of the method. In the current study, the data were then normalized by dividing the measured concentration at a given seat location by this reference concentration:

$$C_{REF}=\frac{C_{AVE}+C_S}{2}, \quad (2)$$

where C_{AVE} is the spatial average concentration over all measurement locations, and C_S is the maximum concentration (occurring usually nearest to the source). Since the cabin air is not well-mixed, inclusion of C_S helps to make C_{REF} more representative of source strength. Conversely, C_{AVE} is included because C_S by itself would introduce too much variability due to near-source anisotropy. Also, C_{AVE} is a reasonable indicator of air change rate. The dimensionless concentration variable used in the analyses is then the ratio of the measured concentration, C_{MEAS} to C_{ERF}:

$$C=\frac{C_{MEAS}}{C_{REF}}. \quad (3)$$

If the measurements are made in the presence of a background concentration, C_0, as was the case with the CO_2 tracer experiments, a more general form of the equation is needed:

$$C=\frac{C_{MEAS}-C_0}{C_{REF}-C_0}. \quad (4)$$

Thus far, the GAATE model has been applied to datasets from the University of Illinois and KSU and also to case study information on the flight from Hong Kong to Beijing on March 15, 2003.

Statistical modeling

The model chosen currently is regression analysis, where the dependent variable is concentration and the independent variable(s) describe location within the cabin. When a linear model was used, the regression equation had the general form

$$Y_i=\beta_0+\beta_1 X_i+\varepsilon_i, \quad (5)$$

where Y_i is the observed quantity (contaminant or pathogen concentration); β_0 and β_1 are, respectively, the *y*-intercept and slope of the regression line; X_i is the independent random variable; and ε_i is the residual for the *i*th observation. Various functional forms were chosen to attempt a fit to the data, by inspecting a plot of concentration versus distance from the source. If a linear model did not fit the data well, exponential regression of the following form was used:

$$Y_i=\beta_0 e^{\beta_1}+\varepsilon_i, \quad (6)$$

where, in this case, the betas are amplitude and decay parameters, and ε_i is still the residual for the *i*th observation. In preliminary analyses, distinguishing between the seat letter coordinate direction and the row number coordinate direction did not provide a better fit than using the simple variable of distance, *r*. Thus, *r* was used as the independent variable throughout the study reported here.

Illinois data

Measurements of carbon dioxide as a tracer gas were taken in a five-row, twin-aisle mock-up. Data were generated over 3 air change rates and 2 source locations to form a complete block of 6 datasets, in which the measured outcome was concentration at each of 35 seat locations. The ventilation rates were 816, 1052, and 1259 m^3/h (479.5, 618.18, and 739.8 cfm), corresponding to 80%, 100%, and 120% of the full ventilation load of a realistic operating condition. The two source locations were seats 2B and 4F. The concentrations measured at 2-s intervals were time-averaged over 1000 s after the system had stabilized. No exhaust air was recirculated, and the gaspers were off. These datasets reflect an isothermal scenario. A CFD simulation was performed for the same set of conditions. These results were not included in the GAATE model, because they did not fit the same regression equation as the experiments, which were considered more reliable. In principle, data generated by CFD are reasonable candidates.

Kansas State data

Kansas State researchers staged three types of contaminant releases, summarized in Table 1: CO_2 tracer gas, talc particles, and aerosolized *Lactococcus lactis*.

Cabin mockup—The aircraft cabin mockup facility used in these studies is located in the Aircraft Cabin Environment Research Laboratory at KSU. It is based on the geometry of a specific airliner but is intended to be representative of a mid-size wide-body aircraft in general. The cabin is 9.45 m (31 ft) long and contains 11 rows of seats. The seat spacing is 825 mm (32.5 in) per row, and the seats are 7 across in a 2–3–2 configuration. The air inlet diffusers are from the actual aircraft as is the air distribution system that supplies the diffusers.

The air supply design for this aircraft consists of two linear slot diffusers extending the length of the cabin near the center ceiling of the cabin, each blowing outward. The inlet airflow is uniform along the length of the cabin. The uniformity of this airflow was experimentally verified for both sides (Mazumdar et al. 2008). Air exits the cabin through continuous floor level exhausts on both sides of the cabin. The mockup is equipped with coach seats from the specific aircraft, and each seat is occupied by a thermal manikin with a heat output of 100 W. The manikins do not breathe or perspire. All inlet air is conditioned and passes through HEPA filtration prior to entering the cabin. There is no recirculation. The total airflow rate to the cabin was 660 L/s (1400 cfm) for all data presented.

Description of experiments—The first set of experiments used carbon dioxide (CO_2) tracer gas to measure contaminant dispersion. The CO_2 tracer gas was mixed with helium (He) to generate a mixture with density equal to that of air. The tracer gas was at the same temperature as the cabin air when injected. Since CO_2 is much denser than air, negative plume buoyancy results in distorted results if these measures are not taken to ensure neutral buoyancy. Calculations and experimental results show that turbulent diffusion is several orders of magnitude greater that molecular diffusion, so the molecular diffusion is expected to be a negligible consideration in these experiments. The tracer gas was injected continuously at low velocity through a vertical tube in the center of either the right or left aisle at a height of 1.2 m (48 in) at row 6.

The air was sampled through a seven-port sample tree. All measurements reported are at a height of 1.5 m (60 in.). Air was sampled from one port at a time for a minimum of 30 min before proceeding to the next port. Once all ports were sampled, the entire tree was moved to the next location.

The second set of measurements use talcum powder as a representative solid particle contaminant (Beneke et al. 2011). The peak number density for this powder occurred at approximately 1.5 μm, and the data presented are for the total particle numbers between 0.5 and 5.0 μm. Injecting solid particles in a controlled manner without disrupting the cabin airflow is difficult. In order to accomplish this feat, a “puff generator” was developed. A measured amount of talcum powder was placed in a small cup. A small copper tube connected to a source of pressurized air was directed downward at the cup. The airflow was turned on and off very quickly by a solenoid valve to generate a very short but intense puff

of air that aerosolized the talcum powder without generating any large airflow. Figure 3 shows seven of the devices being tested simultaneously.

For the experiments, the injection occurred in row 2 and was injected simultaneously at all seven seats in the row. Particle concentration was measured using an optical particle counter with the instrument placed in the seat, as shown in Figure 3. A straight tube was used to collect air samples at a height of 1.18 m (46.5 in.). Prior to injecting the talcum powder, aerodynamic particle sizers (APSs) were monitored to verify that the air was free of particles and the count rate near zero. Data were then collected for 15 min after injection at which time the counts had returned to near zero. The data reported here are the 15-min sums.

The third set of measurements used aerosolized *Lactococcus lactis* as a surrogate bacteria. The bacteria were aerosolized using a handheld mister (Figure 4), and the mist was released around head height of the seated “passengers.” Collection plates were located on the top of the seat backs. The collection plates were opened for collection 30 min after the *L. lactis* was released. Controls were also run with no bacteria aerosolized to verify that near zero counts were obtained, and thus, all counts measured could be attributed to the aerosolized *L. lactis*.

Longitudinal dispersion—Again, it is noted that these three sets of experiments were conducted with different distributed media, and this is the first study comparing the three airborne contaminant types.

For the tracer gas measurements, the tracer gas was injected at row 6, and measurements were made along the entire cabin centerline. For the solid particles measurements, the particles were injected at row 2. One APS was located in seat 3D for all experiments and was used as a reference. A second APS was placed, in turn, in each of the D seats for rows 4–11. For the bacteria measurements, the aerosolized bacteria were sprayed along the front of the cabin, generally in the row 1 area (Figure 4). Measurements were taken at each seat, but, for the purpose of this study, only the data for the three center seats are reported.

Lateral dispersion—The injection for the tracer gas and for the solid particles is the same as for the longitudinal dispersion. Tracer gas measurements were made from side-to-side for rows 5–9. For the particles, measurements were only made in rows 4 and 7. For the bacteria, releases were made at seats 6B, 6D, and 6F, and measurements were collected at all seats. The lateral dispersion results for the bacteria release were not included in the GAATE model because of the difficulty in assigning a source-receptor distance.

Results

Illinois

The specific form of Equation 5 that provided the best fit to the experimental tracer gas data was

$$C=\beta_0+\beta_1 \ln\left(\frac{1}{r}\right). \quad (7)$$

The regression line shown in Figure 5 has an intercept, β_0, of 1.055 and a slope, β_1, of 0.493. With an R^2 value of 0.476, it can be said that 47.6% of the variability in the concentration data is explained by the regression model. While the regression passed the normality test ($P = 0.141$), it failed the constant variance test, which is not surprising given that the concentration varied much more near the source.

The analysis resulted in the regression line and error bars shown in Figure 5. Error or uncertainty applies here in two different ways. β_0 and β_1 each have 95% confidence intervals, $[0.9906 \leq \beta_0 \leq 1.1194]$ and $[0.4204 \leq \beta_1 \leq 0.5660]$, and these intervals are not independent, which is why the blue confidence bands are curved. The red bands indicate the uncertainty in the prediction of the $C \sim \ln(1/r)$ relation for any member of the population of r values. Put another way, the confidence band (blue) addresses the question of whether this regression line is the best one possible, while the prediction band (red) addresses the value of this regression line as a predictive model.

Because the concentration variability is greater nearer the source, a two-segment linear regression was also done to see if the fit could be improved (Figure 6). The slopes of the two lines and the breakpoint between them, $r = 2.48$ m, were both determined in the regression. Thus, a physicality—the near-zone/far-zone distinction—was identified by the statistical analysis. The freedom to adjust for this phenomenon increased the R^2 value from 0.476 to 0.502, which is only a small improvement. Here also, the analysis passed the normality test ($P = 0.375$) but failed the constant variance test. The near-source behavior is perhaps not well described by any kind of model based on the isotropic assumption. However, performing the regression on only the far-field data—greater than 2.48 m from the source—actually lowered the R^2 value. The benefit of more data points was apparently greater than the cost of the increased variance.

KSU

The regression analysis of the KSU tracer gas data was the least successful of the modeling attempts, with an R^2 value of 0.317. The large variability near the source suggests that grouping the data might show a trend more clearly. In Figure 7, the distance variable has been discretized into five bins of $0 < D \leq 1, \ldots, 4 < D \leq 5$ and assigned distance values of 0.5,… 4.5 m. Also, only the mean concentrations are plotted for each bin. These summarized data fit the curve very well, with an R^2 value of 0.988. However, because the variability around the mean has been removed from the analysis, the good fit requires circumspection. Interestingly, the best-fit model equation did not change very much between the two analyses, where the regression models were

$$C = 916\exp(-0.136r) \quad (8)$$

and

$$C = 999\exp(-0.152r) \quad (9)$$

for the individual and averaged data series, respectively.

The KSU aerosolized bacteria release followed a two-segment linear regression model better than any other equation form, even though the R^2 value of 0.685 did not indicate an especially good fit. Figure 8 shows the statistically determined breakpoint between near and far fields as 2.56 m, which is quite close to the 2.48 m found in the Illinois tracer gas data. Also apparent in the plot is the large near-field variability, which is responsible for most of the deviation from the model.

Of the three contaminant types, the talc particle data was the most explainable using a regression model on distance. An exponential decay equation,

$$C = 14,150 \exp(-0.487r), \quad (10)$$

fit the particle counts with an R^2 value of 0.778. The relatively good fit shown in Figure 9 might be attributable to the scarcity of measurements close to the source.

With all KSU data combined and normalized by Equation 3, the large number of observations and the varying distributions in the contaminant trials create together a fit that is somewhat impressive in its generality but also limited in its explanation of observed variability. Equation 11 fit the large dataset with an R^2 value of 0.614, indicating that the GAATE model concept is potentially useful:

$$C = 1.75 \exp(-0.710r). \quad (11)$$

In-flight SARS case study

The case study data differed from the experiments in several important ways. The data come from real cases of infection, the aircraft is single-aisle rather than twin-aisle, and the outcome is a binary rather than a continuous variable (Olsen et al. 2003). The fact that the data document real infection provides tremendous value, while the single-aisle aircraft configuration represents a source of unmodeled variability (i.e., error). Contracting or not contracting SARS is a binary variable that was transformed into intermediate fractional values by counting the infection rate in a group of seats.

Thus, the dependent random variable was the number of cases in a seat row divided by the total number of passengers in that row, e.g., 1/6. The independent random variable in the model was row distance. This was defined as the absolute difference between the number of the row of interest minus the number of the index passenger's row. In other words, simply the distance measured in rows (Figure 10). Because the index passenger was assumed to breathe, cough, or sneeze in the forward direction, a one-row offset was applied so that the row in front of the index row became the effective source location.

A three-row grouping was also analyzed in an effort to make the infection rate closer still to a continuous variable and to smooth the step-function variability in infection between adjacent passengers that might be expected due to individual susceptibility. The grouping approach might have been taken with the experimental data as well, but some distance information would have been lost. For the real disease cases, the near-field distance information is probably too noisy to be valuable.

The real flight case study data showed a decrease in disease incidence with distance in a manner similar to the concentration decrease with distance seen in the experiments with various contaminant types. The decrease in SARS incidence with increasing row distance was fitted to a linear regression line:

$$I=0.297-0.0295D, \quad (12)$$

where I is the infection rate, and D is the distance, measured in rows rather than meters. This model accounts for approximately 61% of the variability in the data, as the R^2 value is 0.612. The model line intersects the y-axis (zero distance, D) at an infection rate of approximately 30% of passengers and reaches zero incidence at a distance of ten rows. Note that this infection-rate/source-distance model behaves as well as the combined KSU experimental data model, with R^2 values each of 0.61.

The model fit improves modestly to 0.640 if the row in front of the index passenger is designated the source row as an accounting for the forward momentum of a cough or sneeze. However, the local variability still is hard to model. A symmetric grouping of rows that includes one row ahead and behind the source row and the row itself results, understandably, in a much better fit, with an R^2 value of 0.887. Better still is the three-row grouping combined with the one-row offset, plotted in Figure 11. The regression line is

$$I=0.0438D+0.370. \quad (13)$$

Discussion

Once a concentration–space relation is established, it can be applied in useful ways. With at least half the variability being explained by distance from the source, estimation using these simple models is widely applicable in the cabin environment, though the predictive power has quantifiable limitations. An interactive graphical tool was built using the idea that the relative exposure, taken here as the time average of normalized concentration, can be estimated for a source located anywhere in the coach section. Figure 12 shows this idea actualized with a program written using software that supports simple graphical tool development. By clicking on any seat in the cabin diagram, the exposure is calculated for the rest of the ten-row field. The figure is an example of the resultant field from one source location.

Such an exposure map can be used to refine assumptions made about how far air contaminants, such as small droplets, travel in the cabin. Also, a case history and an exposure map may be used together to gauge infectivity by the airborne route. Moreover, infectivity and relative exposure can support decisions about which passengers should be contacted for follow-up after a reportable disease incident. The concept of seating distance from an index patient was used during investigation of rubella exposure on several flights in June of 2008 (Kim et al. 2012). While the authors indicated typical contact follow-up zones as being the index patient’s row, two rows in front and two rows behind, lap-help children, and the flight crew, they attempted follow-up in this investigation, additionally, with all passengers who shared a cabin or, for smaller planes, all passengers. They reported that no

passengers in the comprehensive follow-up (86% of all passengers) showed evidence of rubella infection. They interpreted this result as supporting the adequacy of the customary protocol, although they acknowledged that most passengers were found to be already immune from rubella through vaccination records, serologic testing, or age.

Clearly, airborne exposure is only one piece of the puzzle. Kim et al. (2012) noted that of the three passengers that were considered susceptible to rubella, one was seated four rows in front of the index patient on a short domestic flight, and two were seated six and seven rows in front of this index patient on an international flight. Without a passenger distance exposure metric, it is difficult to know where four rows on a short flight or seven rows on a long flight lie on the continuum of cabin exposures. Considering SARS, Table 2 shows that the infection rate had decreased by 90% at a distance of approximately eight rows. Even though SARS is a different pathogen, this model suggests that a rubella-susceptible individual on the longer flight could have become infected if seated significantly closer to the index patient. It may be worth considering that the index patient row distances of three, four, and five are beyond the customary contact follow-up distance while being closer to the index patient than the closest susceptible passenger (six rows) on the international flight in Kim et al. (2012).

For the exposure map to be useful, it must be reliable to some degree. In other words, the GAATE model must do a decent job of quantifying exposure risk and uncertainty. The five datasets presented here have moved the model in the direction of reliability; exactly how far is difficult to know. As the number of data points increases, so does the variability. Statistical power to draw inferences from a dataset can be thought of as the balance between the size of a data set (N) and the variance (σ^2) it contains. Power increases as N increases and as σ^2 decreases.

It is important to acknowledge that data were collected only in coach-class cabins, which typically contain large numbers of rows. Longitudinal dispersion in first-class cabins, which have far fewer rows and are bounded by bulkheads and perhaps a closed curtain, is likely to be quite different, although the nature of the difference is not intuitively obvious. For example, the bulkhead could act as a boundary to longitudinal flow and thus promote contaminant mixing, or the bulkhead surface could act as a contaminant sink. Larger row distance and fewer passengers/thermal plumes would also affect the flow field.

Interactive graphical tool

The use of an independent variable as simple as distance from a source facilitates visualization of model predictions as an exposure estimation map on the cabin topology. Realization of this idea is a tool that estimates exposure relative to other passengers, when the cabin contains a source of airborne contamination, such as an index case passenger. Because the tool uses a single regression equation, it can easily be programmed to visualize any of the datasets. The example shown in Figure 12 is based on the Illinois tracer gas data and an index passenger in seat 32B, although the user can specify any seat in the cabin as the source. Naturally, as more data become available, new regression equations can be fitted to regression models and adopted into the program.

Given the four types of data presented here, it is useful to consider what information might be drawn out of these data about risk of exposure to disease-bearing pathogens in aircraft cabin air. The type of data providing the most dispersive infection risk estimate is the tracer gas experiments. Gases diffuse more readily than droplets, and viability does not apply in the measurement.

Differences in the Illinois and Kansas State CO_2 data arise from differences in airflow pattern in the two mockups, even though they are each equipped with real ventilation systems from the represented aircraft. Instantaneous fluctuations in indoor airflows are the norm, but even time-averaged or Reynolds-averaged flow variables are likely to vary under boundary and initial conditions designed to be the same in an experiment. Small variations in diffuser geometry can have a large downstream effect on the macro flow pattern. The number of seat rows in the mock-up is probably an important variable, as a slow circulation was observed during visualization smoke trials in the 11-row cabin at Kansas State that would have been suppressed in the 5-row cabin at Illinois, if the boundary conditions there had even generated a flow that would contain this pattern. The Coriolis force has also been suggested as a possible driver of the very slow clockwise rotation.

Even without a rotation that resulted in spreading the contaminant forward on the port side and aft on the starboard side, the more gradual decrease with distance for the KSU data (Figure 7) may be explainable. While the Kansas State experiments used a neutrally-buoyant CO_2-He mixture, the Illinois work used a dilute CO_2 mixture, which is heavier than air. Thus, the Illinois tracer gas data represents a contaminant with a settling velocity. It is worth noting that the distance at which the model predicts a 90% decrease in concentration is similar for the Illinois CO_2 (6.86 m) and Kansas State particle (6.77 m) datasets.

The particle data is possibly a good indicator of the dispersion of virus-bearing droplets, after they have evaporated into smaller infectious material nuclei with low settling velocities. While viability is not an applicable concept for the talc particles, viruses do not seem to die in air as quickly as bacteria do (Grinshpun et al. 2007).

As CO_2 tracer gas bracketed on the dispersive side, bracketing on the least dispersive and least viable side, the infecting behavior of virus-bearing particles is the release of a bacterialaden water droplet aerosol and subsequent growth on agar plates. Limited viability makes this experiment conservative in the estimation of cabin infection as a function of distance from a passenger source.

To quantify this idea, Table 2 shows the concentration (C) in the fitted models at 1 m (D_1) and the distance at which the concentration was reduced by a factor of 10 (D_2).

However, real infection information is available for SARS transmission during flight. The good fit to a linear model of the rate of SARS infection versus row distance from the index passenger is interesting. No other dataset—not gas, particles, or bacteria-laden droplets—fit a straight line very well. It is possible that the passengers' thermal plumes and respiration enhanced the longitudinal mixing and decreased the rate of concentration decay with distance, thus creating a linear rather than an exponential decrease.

From inspection of the D_2 parameter in Table 2, the Illinois tracer gas, KSU particle, and in-flight data show similar distances at which the exposure metric has decreased 90% compared to what it was at 1, 6.86. 6.71, and 6.36 m, respectively.

The KSU tracer gas data had a low R^2 value (0.317), while the grouped and offset flight data had a very high R^2 value (0.969). While the low R^2 takes validity away from the estimation of contaminant transport behavior, a consistent observation in the current work is that, as data were grouped or averaged to reduce near-field "noise," the predictive equation remained fairly constant while the goodness-of-fit increased dramatically. Thus, the grouped/averaged KSU tracer data had an R^2 value of 0.988, and the 90% exposure reduction distance given by the regression equation was 16.1 instead of 19.3 m.

The linear fit of the in-flight case data suggests that airborne transmission was a path of SARS transmission. If the infecting exposure had been from large projectile droplets only, the disease pattern would have been less symmetric fore and aft. While momentum does play a role, as seen in the improved fit if the row in front of the index passenger's row is considered the source row, the behavior is that when the particle stopping distance is reached, the smaller particles remain in the air to mix. Also, if fomites had been the only route, more of a step function drop off in cases would have been observed, since the likelihood of contacting contaminated surfaces drops off very rapidly outside of the source row.

Conclusion

The ability of the GAATE model to make a contribution during the response to an airborne disease outbreak depends on its predictive power. Improvements in accuracy may come from inclusion of additional datasets. Fortunately, the scalability inherent in this approach paves the way to study additional aircraft types, while the models reported here are best suited to the aircraft type in which data were collected. Still, it seems plausible that contaminant transport variability among commercial passenger aircraft types is not larger than differences in pathogen infectivity or individual susceptibility. Also, exposure duration affects whether an airborne exposure level leads to infection, and this variable was not addressed in the current study.

Exposure to small droplets and post-evaporation nuclei, even at a source distance of several rows, is readily apparent. The airborne pathway, then, should be considered part of the matrix of possible disease transmission modes in aircraft cabins, unless the pathogen has been proven nonviable in air. The similar behavior observed in the Illinois tracer gas, KSU particle, and in-flight infection data, as a function of source distance, supports the idea that airborne exposure over a distance of several meters is a significant pathway for SARS infection.

Logical next steps are to perform regression analyses on additional datasets, perhaps including CFD-generated data or statistically simulated (synthetic) datasets. This activity should continue to improve the statistical significance of the GAATE model. Incorporation

of datasets from other commercial aircraft types and passenger cabin configurations would be especially useful.

References

Association of Flight Attendants (AFA-WCA). Letter on April 2, 2003 from Christopher J. Witkowski, Director, AFA Air Safety to Dr. Jon Jordan, Federal Air Surgeon, FAA/DOT. 2003. http://www.afacwa.org/default.asp?nc=4884&id=67.

Baker, AJ.; Ericson, SC.; Orzechowski, JA.; Wong, KL.; Garner, RP. Validation for CFD prediction of mass transport in an aircraft passenger cabin. Report DOT/FAA/AM-06/27. Washington, DC: Federal Aviation Administration; 2006. http://www.faa.gov/data research/research/med humanfacs/oamtechreports/2000s/media/200627.pdf.

Baker, AJ.; Taylor, MB.; Winowich, NS.; Heller, MR. Prediction of the distribution of indoor air quality and comfort in aircraft cabins using computational fluid dynamics (CFD). In: Nagda, NL., editor. Air Quality and Comfort in Airliner Cabins, Vol. 1393. West Conshohocken, PA: American Society for Testing and Materials; 2000. p. 117-134.

Beneke JM, Jones BW, Hosni MH. Fine particle dispersion in a commercial aircraft cabin. HVAC&R Research. 2011; 17:107–117.

Grajewski B, Waters M, Whelan EA, Bloom TF. Radiation dose estimation for epidemiologic studies of flight attendants. American Journal of Industrial Medicine. 2002; 41:27–37. [PubMed: 11757053]

Grinshpun S, Adhikari A, Honda T, Kim KY, Toivola M, Rao KSR, Reponen T. Control of aerosol contaminants in indoor air: Combining the particle concentration reduction with microbial inactivation. Environmental Science and Technology. 2007; 41(2):606–612. [PubMed: 17310729]

Gupta JK, Lin CH, Chen Q. Risk assessment of airborne infectious diseases in aircraft cabins. Indoor Air. 2012; 22:388–395. [PubMed: 22313168]

Hinze, JO. Turbulence. 2nd Ed.. New York: McGraw-Hill; 1975. Chapter One.

Hosni, MH.; Jones, BW. Measurement of airflow in an aircraft cabin using particle imaging velocimety technique. Proceedings of the 4th International Conference on Indoor Air Quality, Ventilation and Energy Conservation in Buildings; October 2–3; Changsha, China. 2001.

Kim C, Chavez P, Pierce A, Murray A, Sander M, Kenyon C, Shrarangpani R, Abernathy E, Icenogle J, Kutty PK, Redd SB, Gallagher K, Neatherlin J, Marienau K. Rubella contact tracing associated with air travel. Travel Medicine and Infectious Disease. 2012; 10:48–51. [PubMed: 22212199]

Lin C, Horstman RH, Ahlers MF, Sedgwick LM, Dunn KH, Topmiller JL, Bennett JS, Wirogo S. Numerical simulation of airflow and airborne pathogen transport in aircraft cabins, Part 1: Numerical simulation of the flow field. ASHRAE Transactions. 2005a; 111(1):755–763.

Lin C, Horstman RH, Ahlers MF, Sedgwick LM, Dunn KH, Topmiller JL, Bennett JS, Wirogo S. Numerical simulation of airflow and airborne pathogen transport in aircraft cabins, Part 2: Numerical simulation of airborne pathogen transport. ASHRAE Transactions. 2005b; 111(1):764–768.

Lin CH, Wu TT, Horstman RH, Lebbin PA, Hosni MH, Jones BW, Beck BT. Comparison of large eddy simulation predictions with particle image velocimetry data for the airflow in a generic cabin model. HVAC&R Research. 2006; 12:935–951.

Liu W, Wen J, Chao J, Yin W, Shen C, Lai D, Lin CH, Liu J, Sun H, Chen Q. Accurate and high-resolution boundary conditions and flow fields in the first-class cabin of an md-82 commercial airliner. Atmospheric Environment. 2012; 56:33–44.

Mazumdar, S.; Priyadarshana, P.; Keshavarz, A.; Chen, Q.; Jones, B. Flow characteristics from air supply diffusers and their effect on airflow and contaminant transport inside an aircraft cabin. Proceedings of the 11th International Conferences on Indoor Air Quality and Climate, Indoor Air; August 17–22; Copenhagen, Denmark. 2008.

Mazumdar S, Poussou SB, Lin CH, Isukapalli SS, Plesniak MW, Chen Q. Impact of scaling and body movement on contaminant transport in airliner cabins. Atmospheric Environment. 2011; 45:6019–6028.

Olsen SJ, Chang HL, Cheung TYY, Tang AFU, Fisk TL, Ooi SPL, Kuo HW, Jiang DDS, Chen KT, Lando J, Hsu KH, Chen TJ, Dowell SF. Transmission of the severe acute respiratory syndrome on aircraft. The New England Journal of Medicine. 2003; 349:2416–2422. [PubMed: 14681507]

Rai AC, Chen Q. Simulations of ozone distributions in an aircraft cabin using computational fluid dynamics. Atmospheric Environment. 2012; 54:348–357.

Sun Y, Zhang Y, Wang A, Topmiller JL, Bennett JS. Experimental characterization of airflows in aircraft cabins—Part I: Experimental system and measurement procedure. ASHRAE Transactions. 2005; 111(2):45–52.

Transportation Research Board of the National Academies. Research on the Transmission of Disease on Aircraft and in Airport: Proceedings 47; 2010. http://onlinepubs.trb.org/onlinepubs/conf/CP47.pdf.

Wang A, Bennett JS, Zhang Y, Dunn KH, Topmiller JL. Tracer study of airborne disease transmission in an aircraft cabin mock-up. ASHRAE Transactions. 2006; 112(2):697–705.

Waters M, Bloom TF, Grajewski B. The NIOSH/FAA Working Women's Health Study: evaluation of the cosmic-radiation exposures of flight attendants. Health Physics. 2000; 79:553–559. [PubMed: 11045529]

Wei Y, Zhang Y, Sun Y, Li D. Experimental and CFD study of unsteady airborne pollutant transport within an aircraft cabin mock-up. Building and Environment. 2009; 44:34–43.

Whelan EA, Grajewski B, Wood E, Kwan L, Nguyen M, Schnorr TM, Knecht EA, Kesner JS. Feasibility issues in reproductive biomonitoring of female flight attendants and teachers. Journal of Occupational and Environmental Medicine. 2002; 44:947–955. [PubMed: 12391774]

Zhang Y, Sun Y, Wang A, Topmiller JL, Bennett JS. Experimental characterization of airflows in aircraft cabins—Part II: Results and research recommendations. ASHRAE Transactions. 2005; 111(2):53–59.

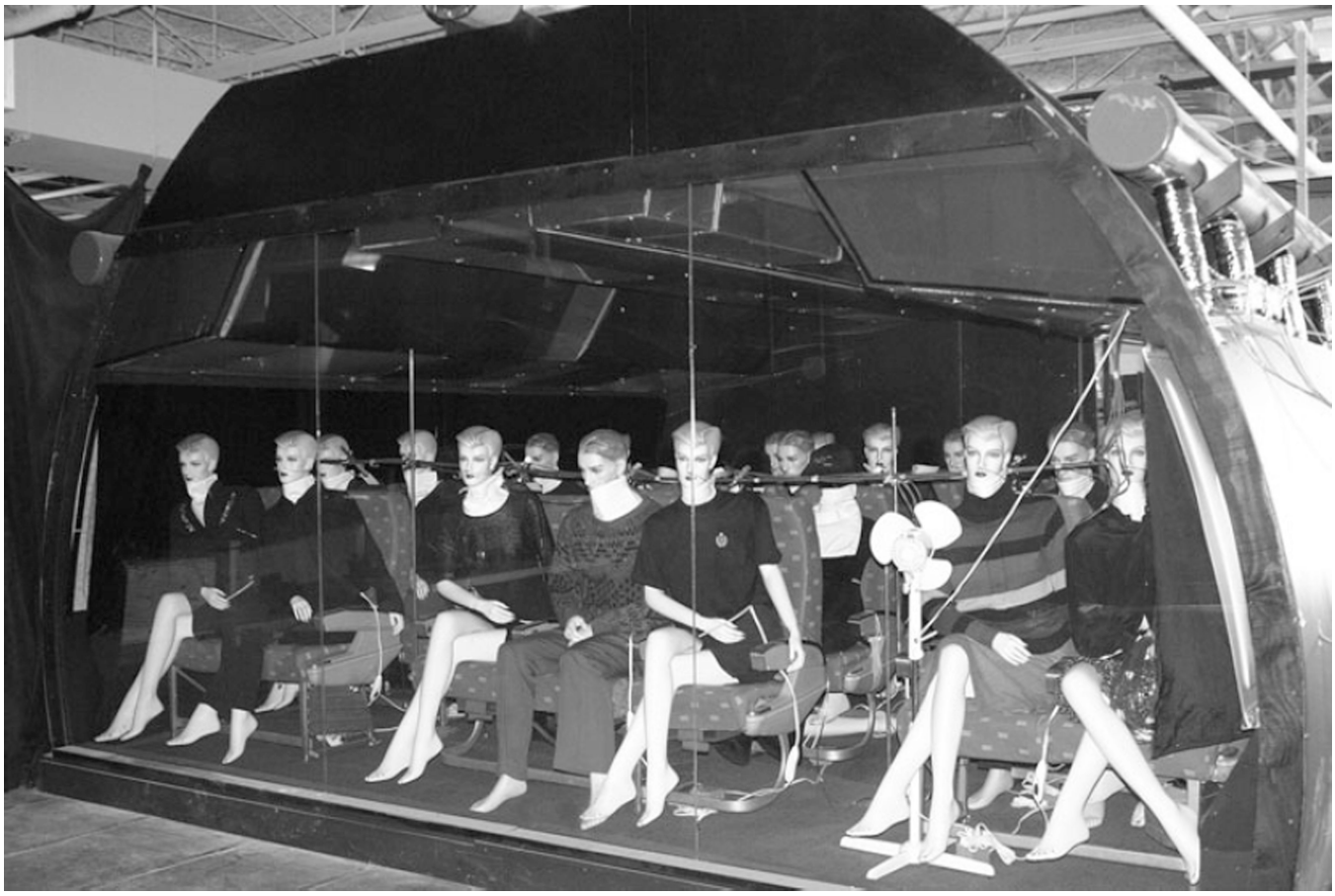

Fig. 1.
B767 mock-up at the University of Illinois.

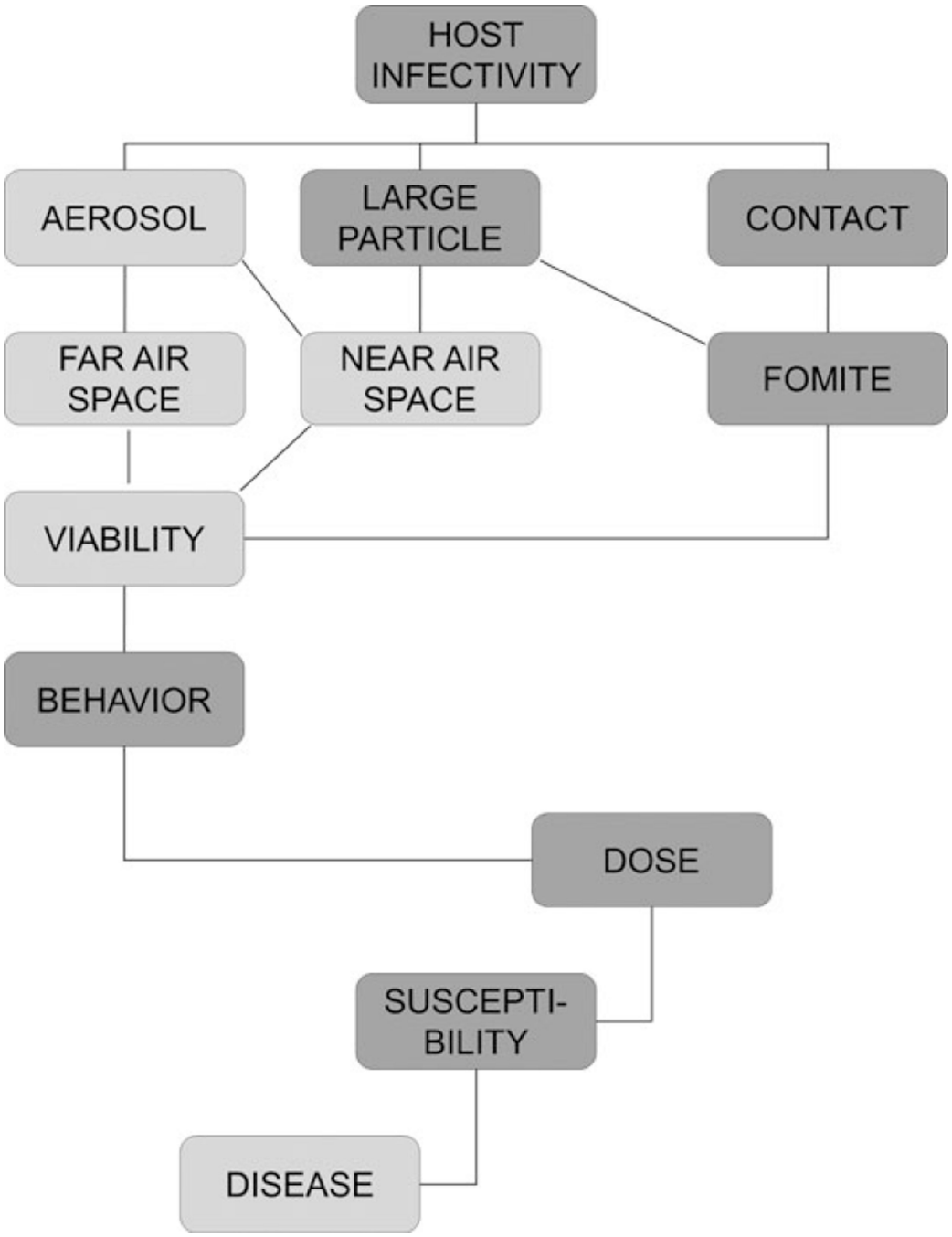

Fig. 2.
Aircraft cabin air quality research (lighter gray) in the context of disease pathways discussed at the 2009 TRB symposium.

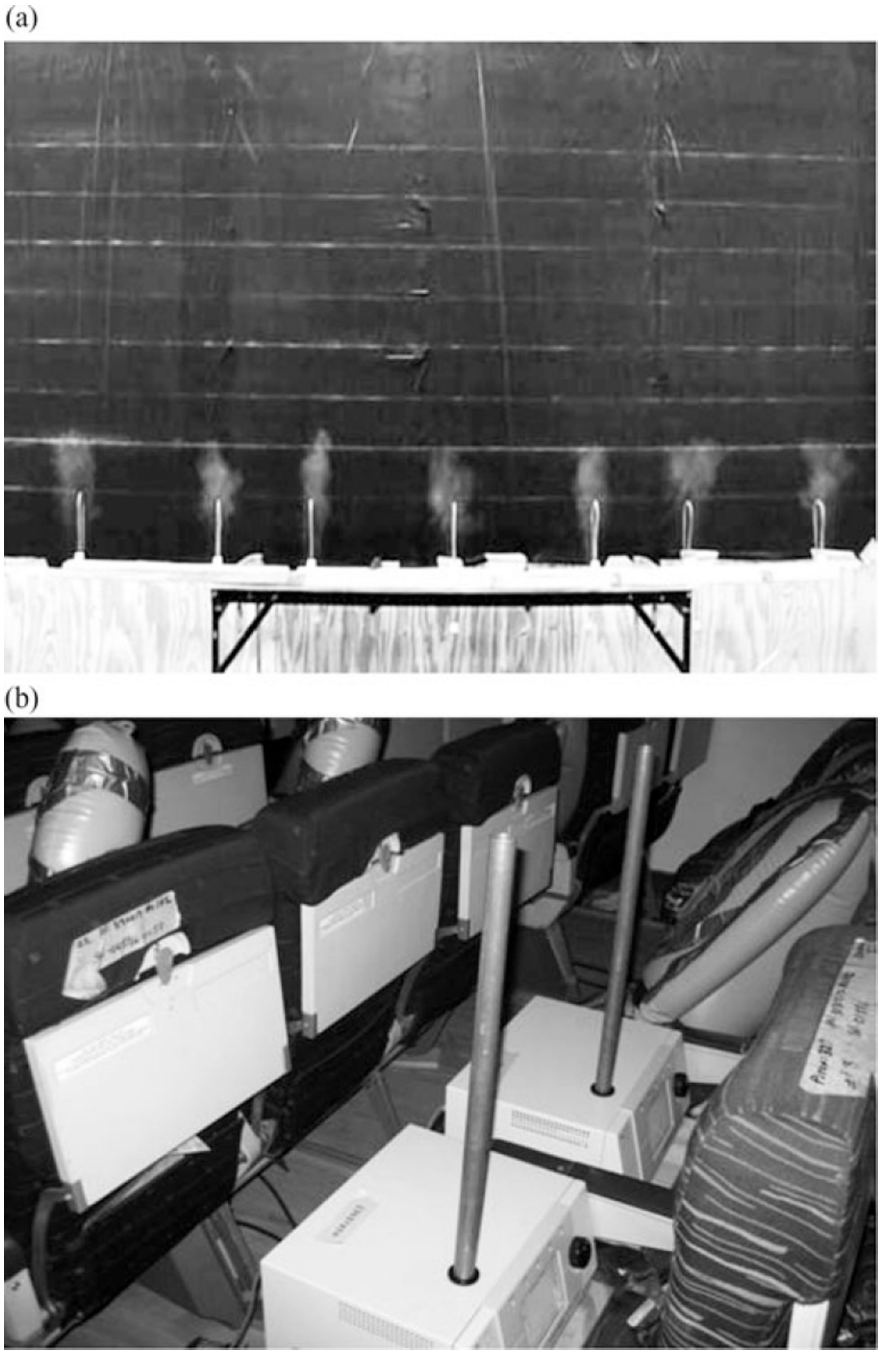

Fig. 3.
Solid particle injection and measurement.

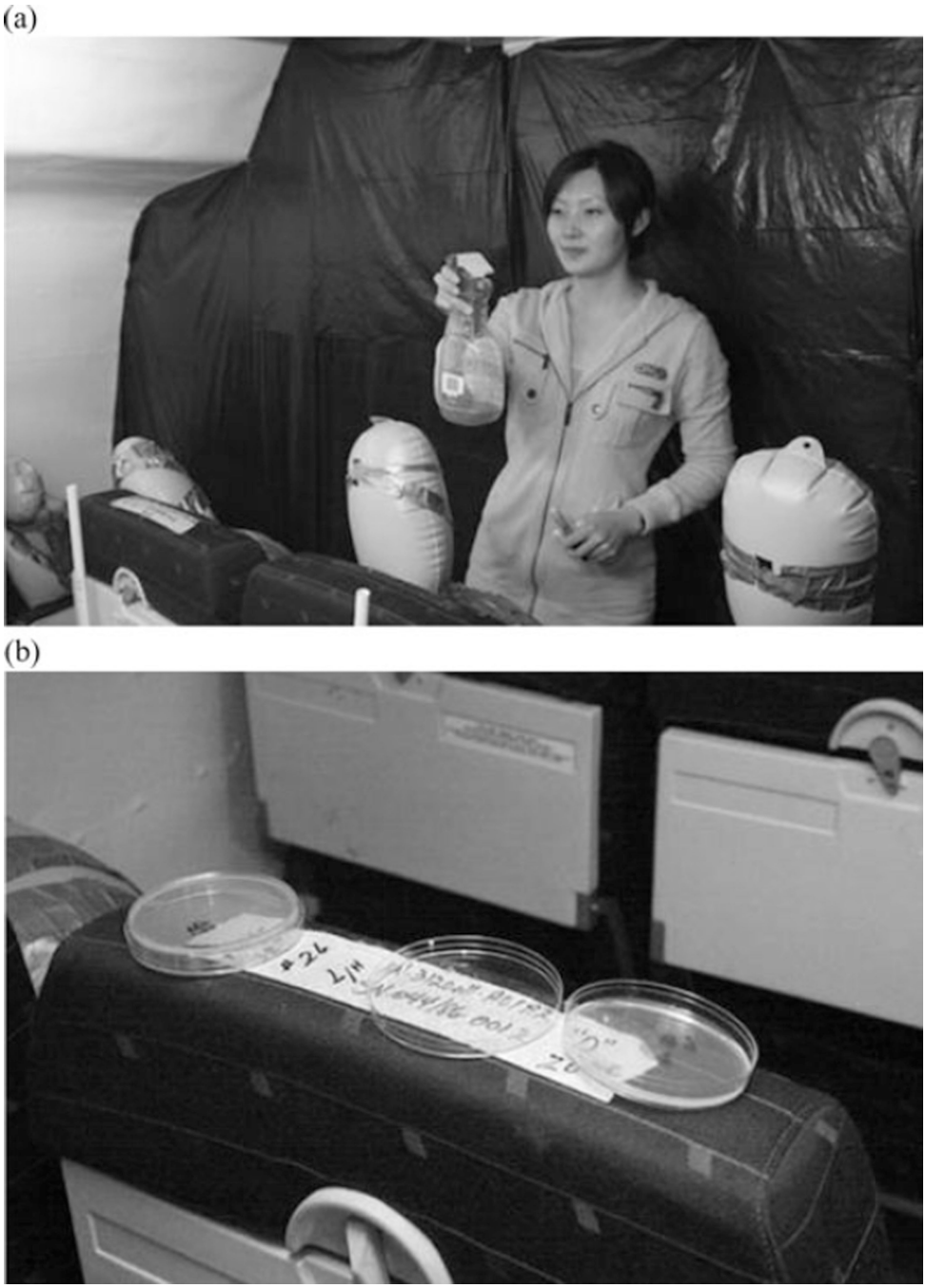

Fig. 4.
Release and collection of bacteria.

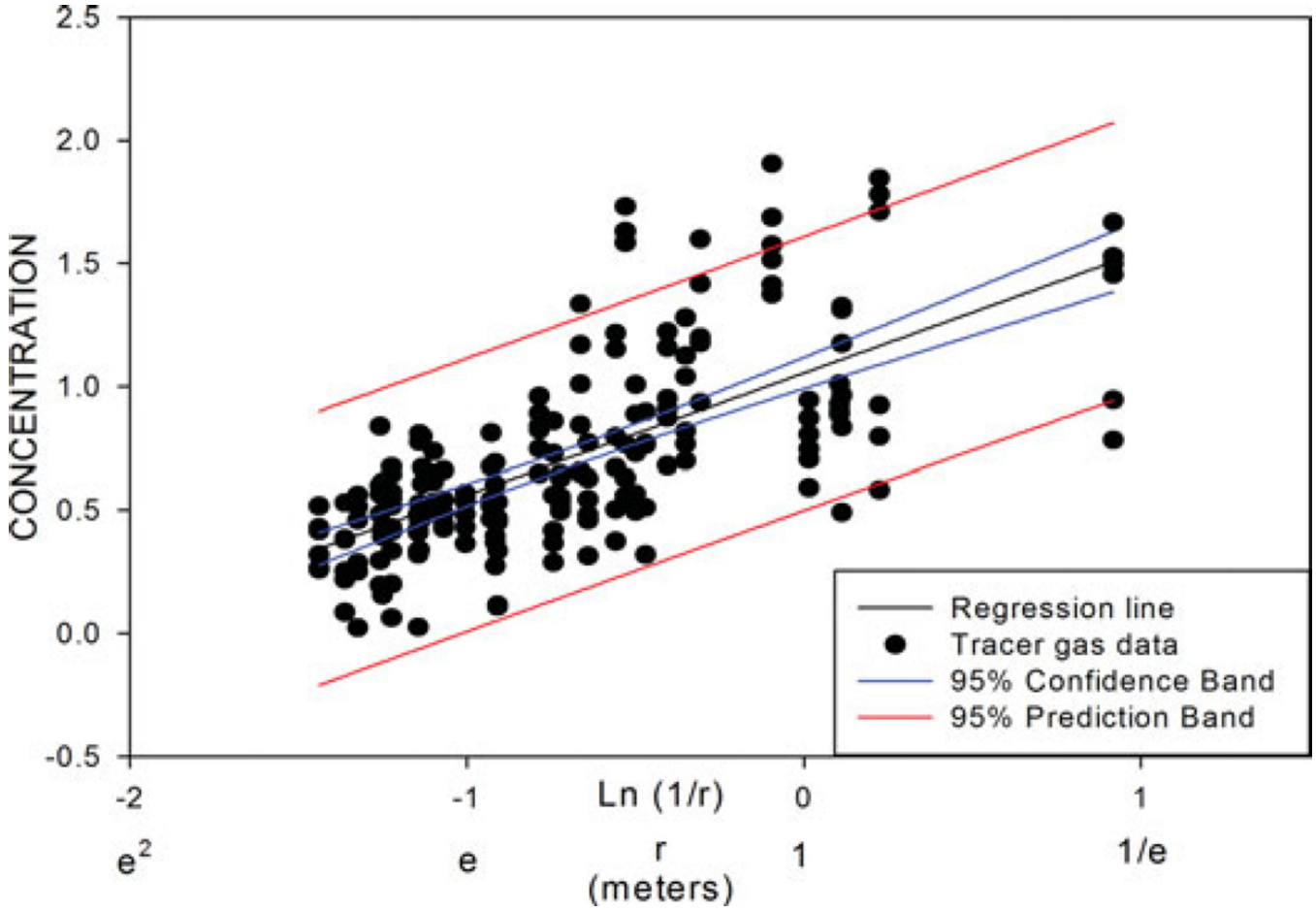

Fig. 5.

Regression analysis of transformed data and 95% confidence and prediction bands (color figure available online).

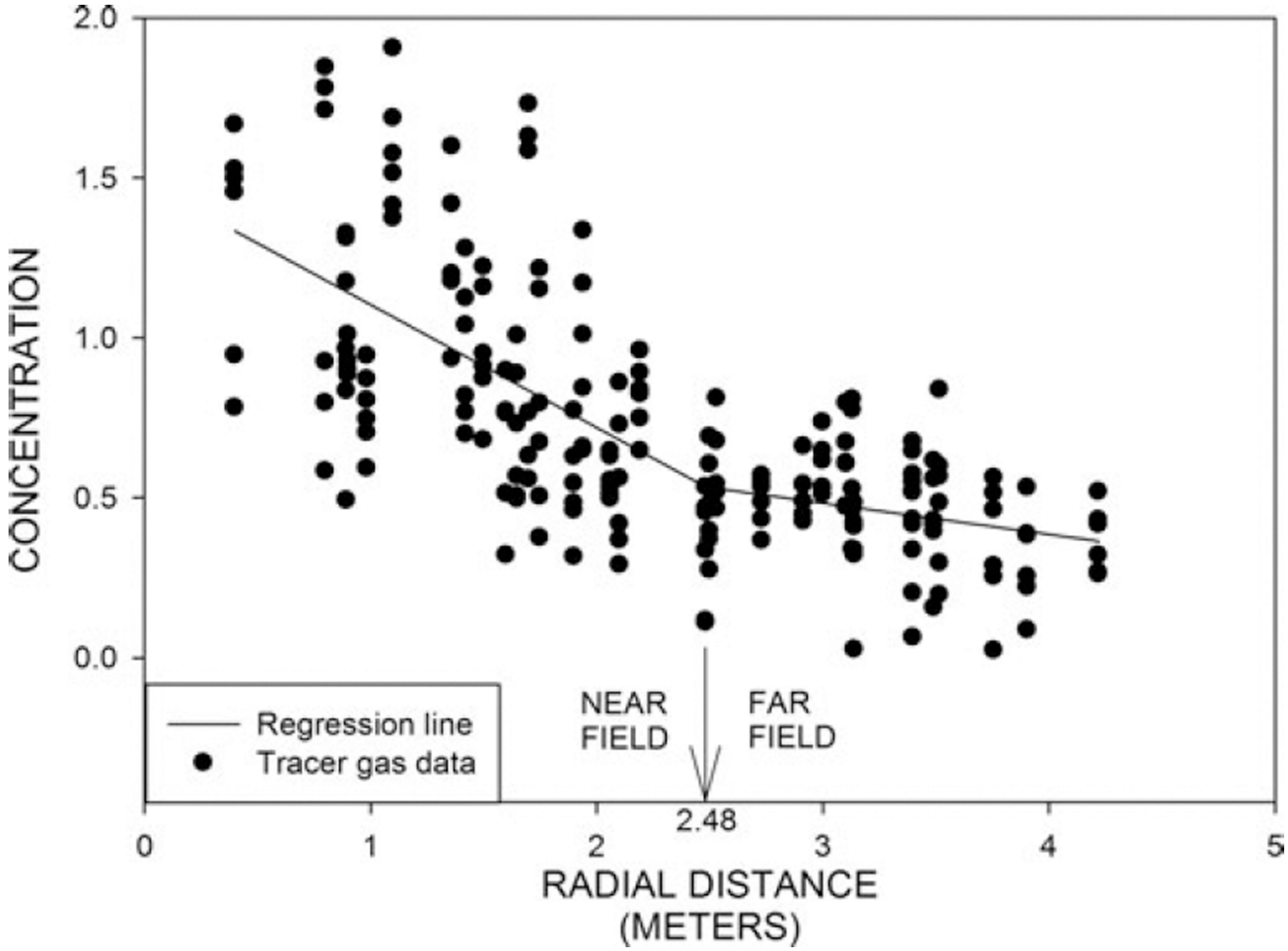

Fig. 6.
Two-segment regression on raw data that shows breakpoint between near and far fields.

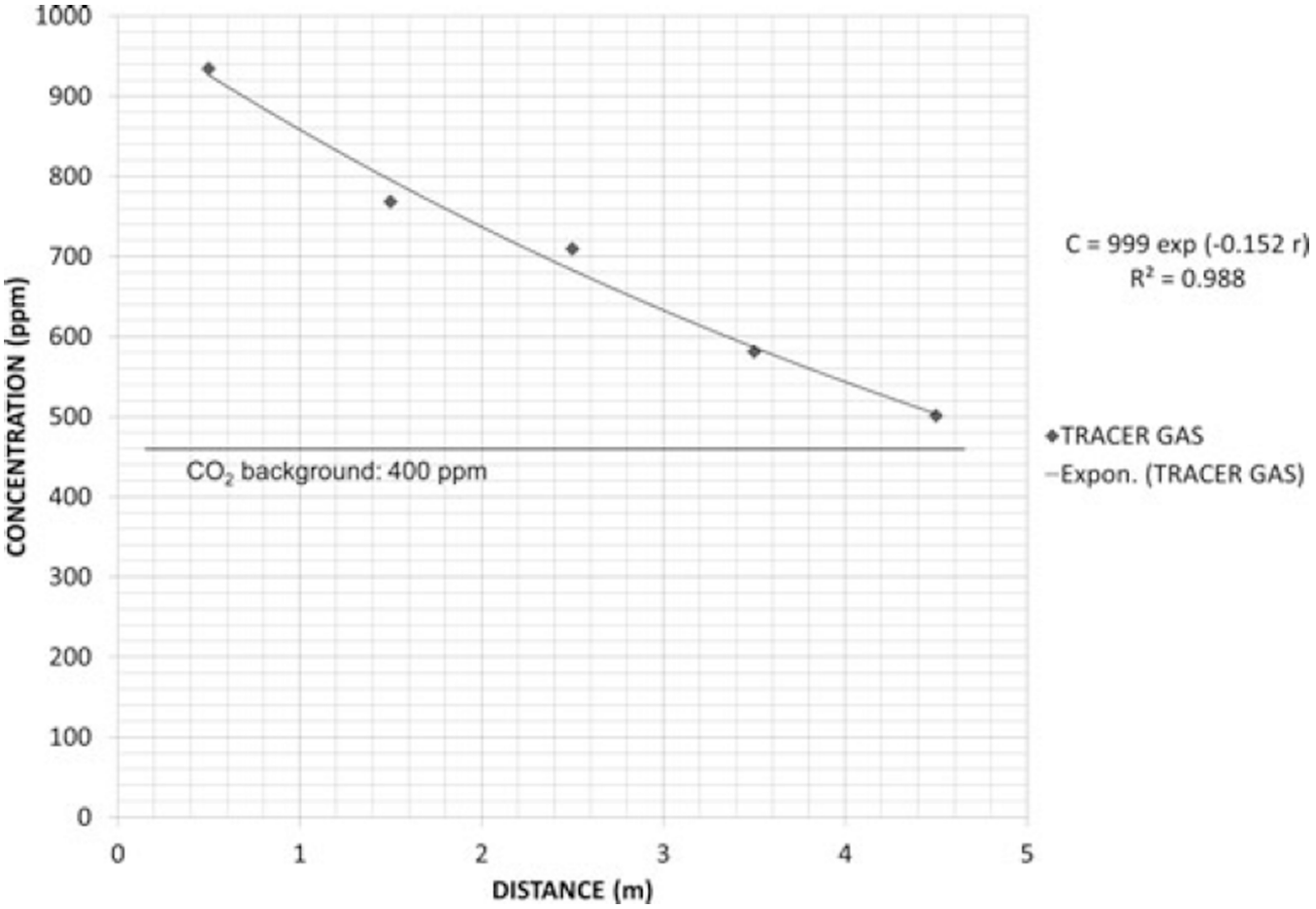

Fig. 7.

Summary data for KSU tracer gas experiments; geometric mean CO_2 concentrations within each distance bin fit a regression model closely.

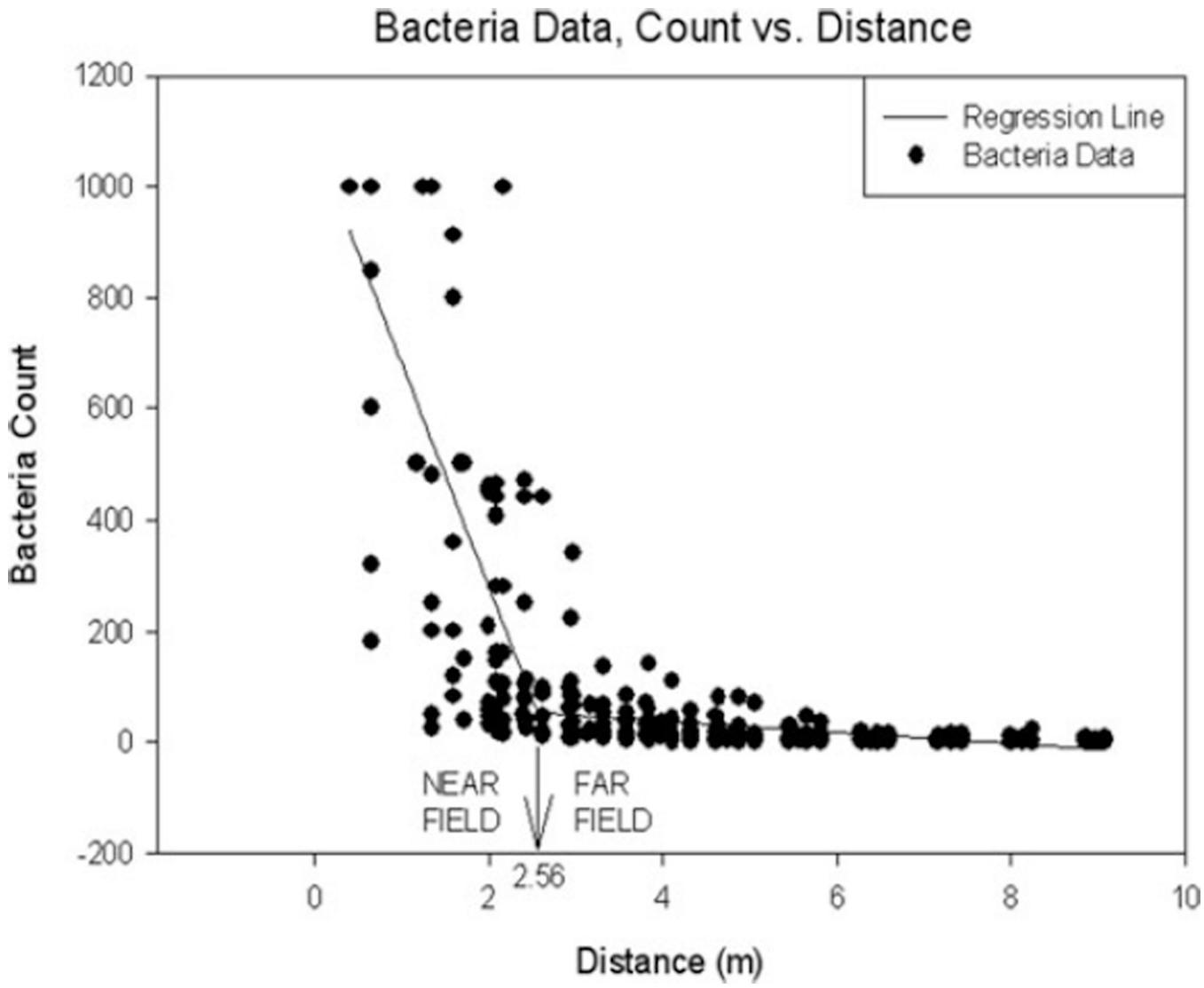

Fig. 8.

Two-segment piecewise regression yielded an R^2 value of 0.685 and a break point of 2.56 m between near and far fields.

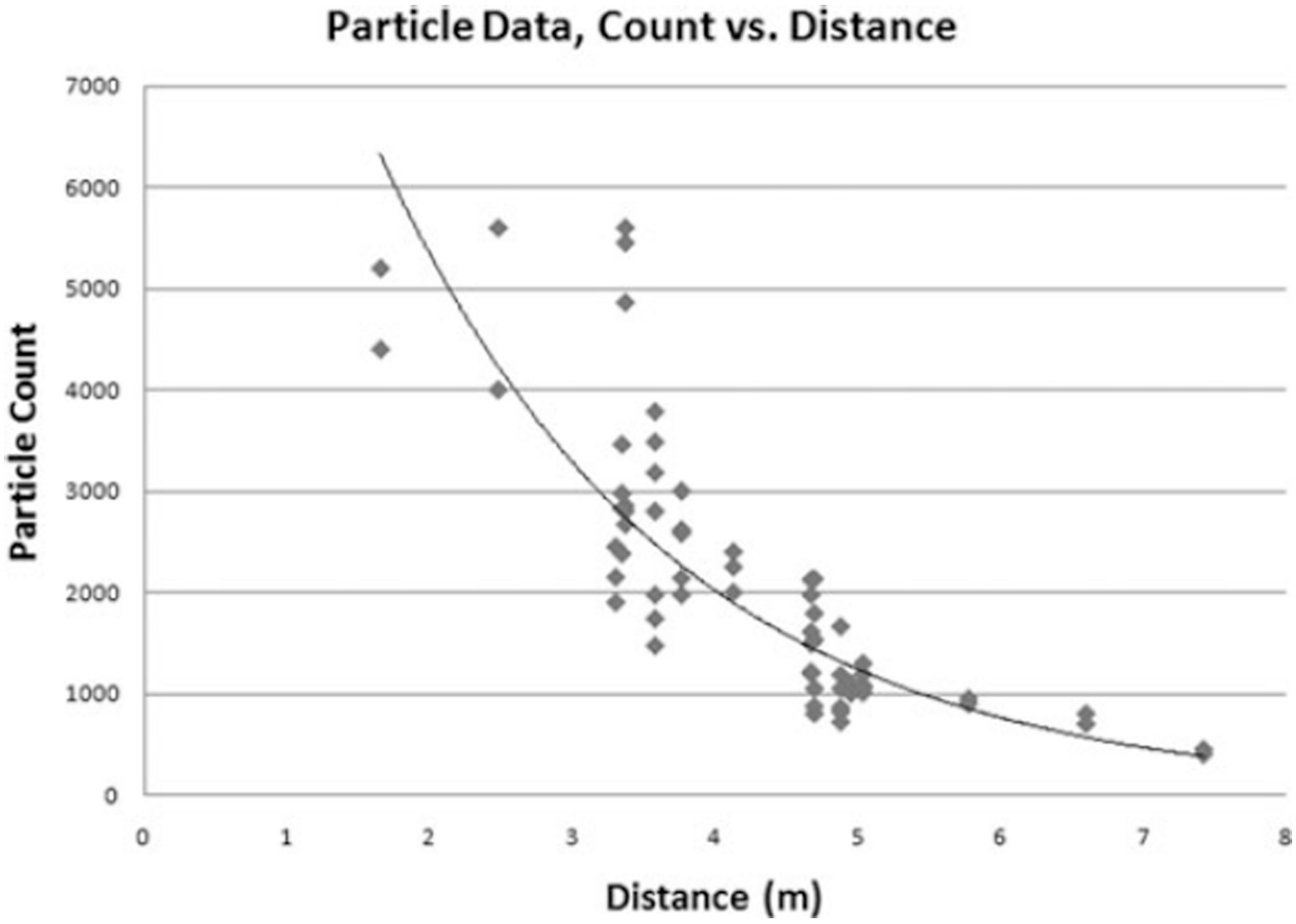

Fig. 9.
Non-linear regression using the model $C = 14{,}150 \exp(-0.487r)$ with R^2 value of 0.778.

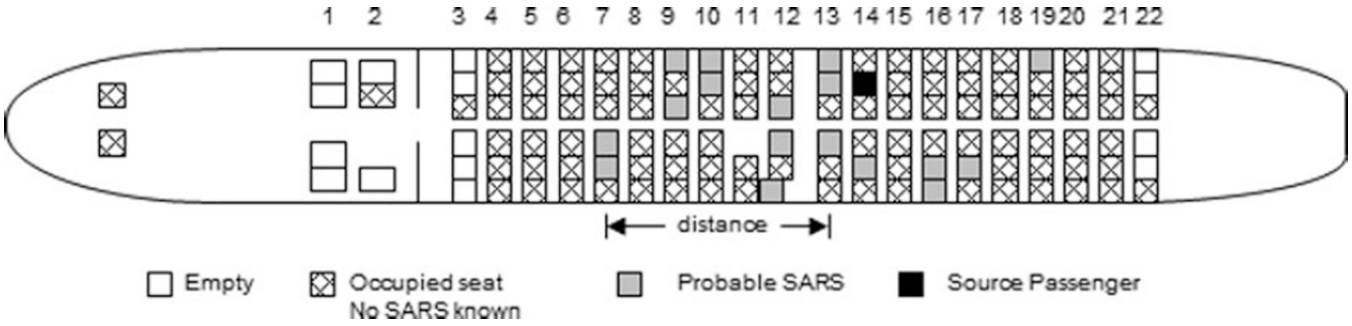

Fig. 10.
SARS cases on China Air flight.

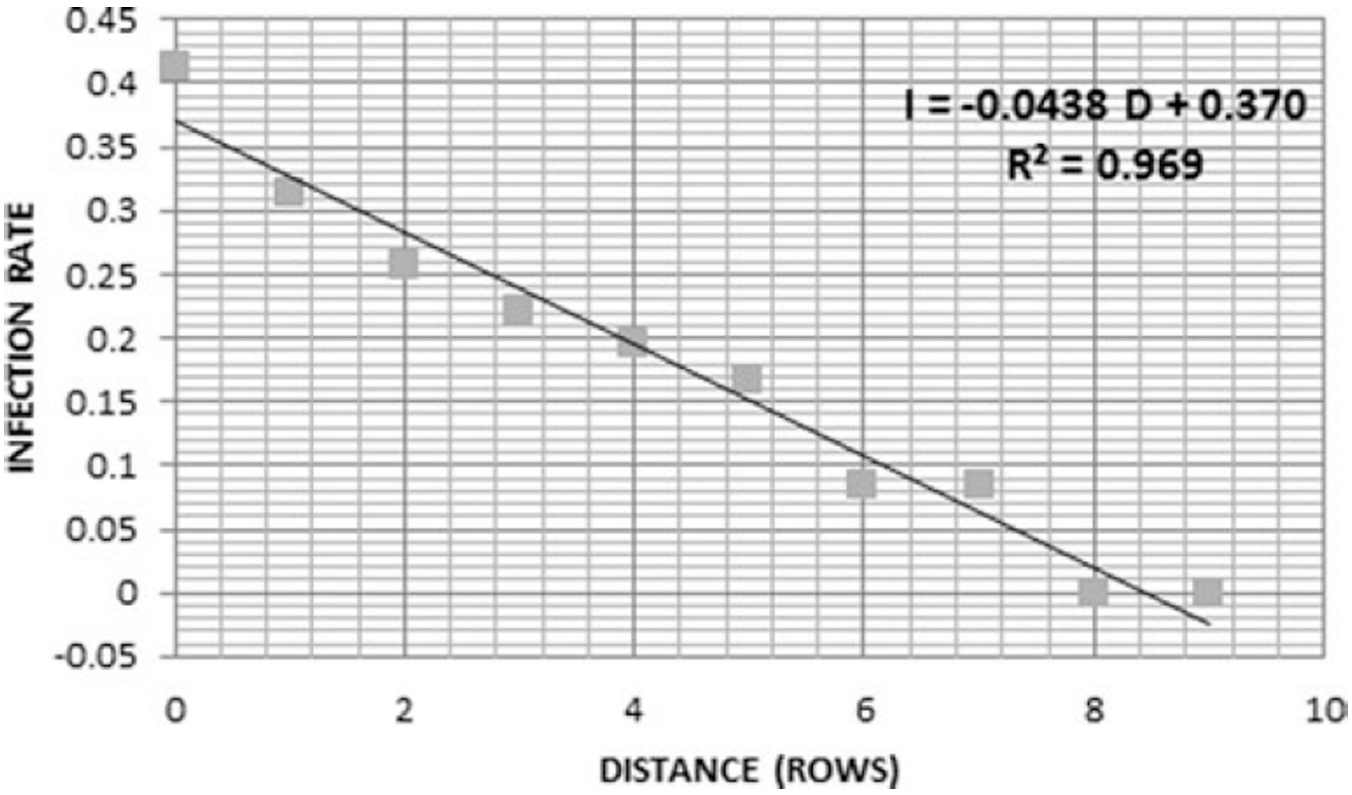

Fig. 11.

Infection rate versus distance measured as rows with a three-row grouping. Row distance is offset to one row in front of index passenger.

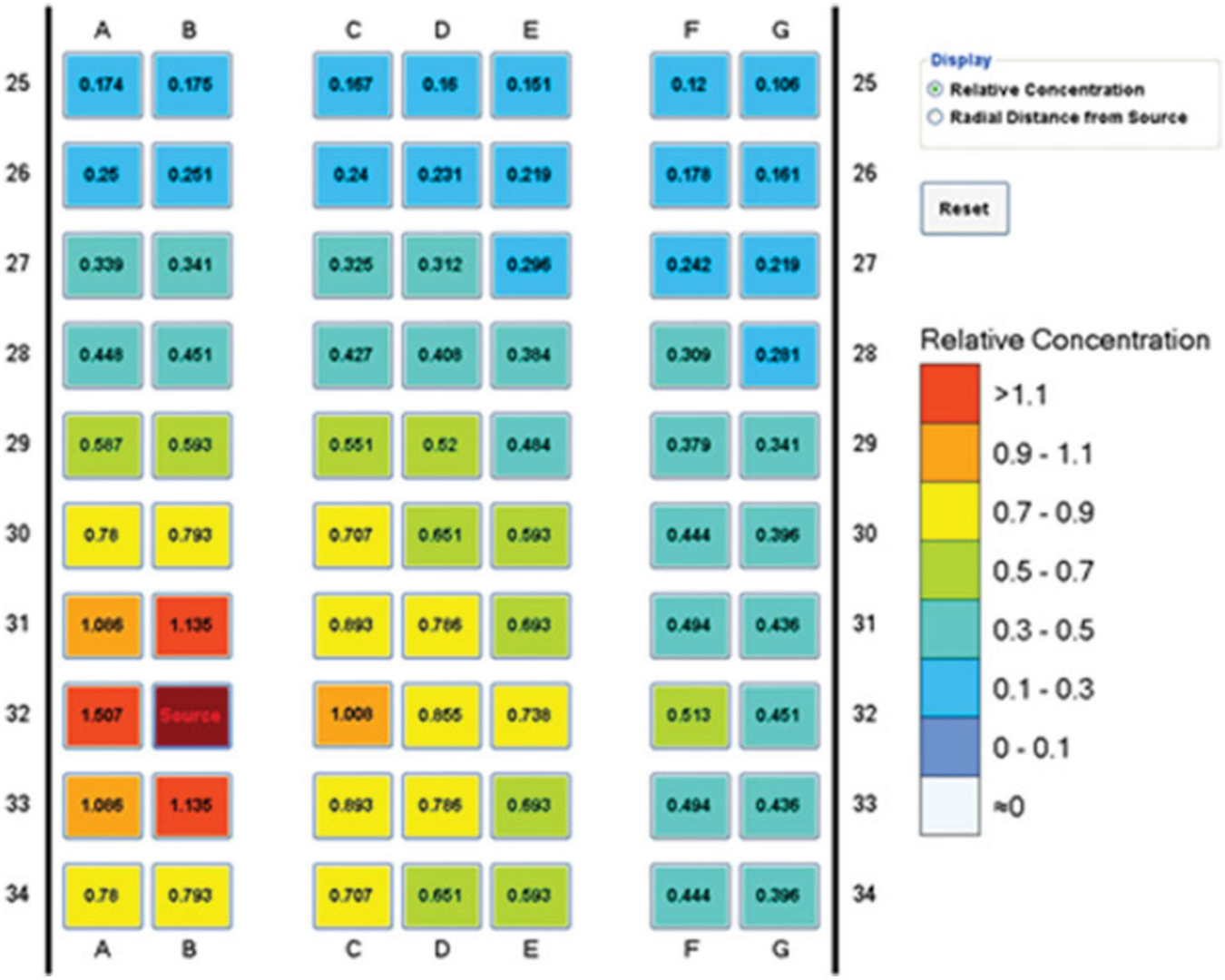

Fig. 12.

Example of use of the GAATE model interactive graphic; relative exposure to an air contaminant from a source in seat 32B (color figure available online).

Table 1

KSU methods summary.

Tracer material	Cabin type	Source description	Ventilation type	Ventilation flow fate, cfm	Sampling equipment	Sampling time, min
Carbon dioxide	Wide-body, twin-aisle	Pressurized tank, diffuser tube located in each aisle at row 6	Isothermal, no recirculation	1400	Non-dispersive infrared sensors	30
Talc particles	Wide-body, twin-aisle	Air pulse release of pre-weighed quantity, emitted in breathing zone of all seats in row 2	Isothermal, no recirculation	1400	APS	15
Aerosolized *Lactococcus lactis*	Wide-body, twin-aisle	Spray bottle used across row 1 at standing breathing zone height	Isothermal, no recirculation	1400	Agar plates, microscopy	30

Table 2

Concentration reduction and distance by model.

Data type	Model	R^2	D_1	C at D_1	10% C	D_2
CO_2 IL	1.055 + 0.493 ln (1/×)	0.476	1	1.06	0.106	6.86 (meters)
CO_2 KSU	916 exp (−0.136×)	0.317	1	667	66.7	19.3 (meters)
CO_2 KSU (grouped)	999 exp (−0.152×)	0.988	1	858	85.8	16.1 (meters)
Particles	14,150 exp (−0.487×)	0.778	1	8695	869.5	6.77 (meters)
Bacteria	422 exp (−0.679×)	0.659	1	214	21.4	4.39 (meters)
Flight	−0.0438× + 0.370	0.970	1	0.33	0.033	7.71 or 6.36 (rows or meters)

HVAC&R Res. Author manuscript; available in PMC 2015 October 30.